NASA CONTRACTOR REPORT

NASA CR-1114

AN EVALUATION OF BORON-POLYMER FILM LAYER COMPOSITES FOR HIGH-PERFORMANCE STRUCTURES

by R. F. Crawford

Prepared by
ASTRO RESEARCH CORPORATION
Santa Barbara, Calif.
for NASA Headquarters

NATIONAL AERONAUTICS AND SPACE ADMINISTRATION • WASHINGTON, D. C. • SEPTEMBER 1968

AN EVALUATION OF BORON-POLYMER FILM LAYER COMPOSITES FOR HIGH-PERFORMANCE STRUCTURES

By R. F. Crawford

Issued by Originator as Report No. ARC R-276

Prepared under Contract No. NAS 7-427, Mod. 3 by
ASTRO RESEARCH CORPORATION
Santa Barbara, Calif.

for NASA Headquarters

NATIONAL AERONAUTICS AND SPACE ADMINISTRATION

For sale by the Clearinghouse for Federal Scientific and Technical Information
Springfield, Virginia 22151 – CFSTI price $3.00

LIST OF SYMBOLS

A	amplitude of initial imperfections in boron layers
B	change in amplitude of initial imperfections due to load
D_B	flexural stiffness of boron layers
d	density
E	Young's modulus of elasticity
$\overline{E}$	effective value of Young's modulus of elasticity
F	factor expressing efficiency of structural geometry
G_M	shearing modulus of matrix material
I	general symbol for structural loading index
K	ratio of effective to actual modulus of boron layer
k_M	foundation modulus provided by matrix
M	moment acting on boron layer per unit width
N	inplane compressive force per unit width
n	exponent in efficiency equation (5)
r	ratio of structural weights, densities, moduli or thicknesses - see Subscripts
t	thickness of constituent layers of composite
V	shearing force per unit width (see Figure 13)
x	coordinates axis
y	coordinate axis; total lateral deflection of boron layer
y_o	initial lateral deflection of boron layer
y_1	change in amplitude of deflection of boron layer due to load

α	ratio of applied load or stress to its critical value
γ	shearing strain of matrix
δ	end shortening of boron layer per wavelength
λ	wavelength of initial imperfections
λ_w	wavelength to minimize critical wrinkling load
ν_B	Poisson's ratio of boron layers
ν_M	Poisson's ratio of matrix layers
σ	stress in the planes of the composite layers
σ_M	direct stress acting on matrix
τ_M	shearing stress acting on matrix
φ_o	see Equation (A38)
φ_s	see Equation (A37)

SUBSCRIPTS

A	shortening due to amplitude A
Al	aluminum
B	boron or shortening due to amplitude B
Be	beryllium
C	composite
CR	critical value
D	density (used only with r)
E	modulus (used only with r)
M	matrix
Mg	magnesium

S	shear, or shearing mode
T	total (used only with δ)
t	thickness (used only with r)
w	wrinkling or symmetric mode of instability

NOTE: Symbols that always appear with a certain subscript are included in the list of symbols and their subscript may not be included here.

INTRODUCTION AND SUMMARY

A composite film of polyimide with boron vacuum-deposited on one side has become available for development as a structural material. The composite film is manufactured by National Research Corporation. The polyimide layer (DuPont H-film) is approximately 0.5 mil thick, and the boron layer is approximately 0.16 mil thick. The objective of the present investigation has been to evaluate the fabricability, mechanical properties, and structural efficiency potentials of this material for structural composites.

Hollow tubular test specimens were readily fabricated by wrapping the composite film over mandrels and bonding layers together with epoxy adhesive. These specimens were then tested under axial and bending loads to determine their stiffness and strength. The test results showed that the effective Young's modulus of the boron layers of the composite was approximately 47.3×10^6 psi; the compressive stress developed in the boron layers was approximately 102 000 psi; and the maximum tensile stress to which those layers were subjected was in the vicinity of 82 000 psi. Because the boron layers constituted about 13 percent of the volume of the composite specimens, the composite stiffness and strength were much less than those of the boron. The polyimide and adhesive contributed low density to the composite properties, but little stiffness or strength.

The mechanical properties exhibited by the boron layers of the film were thus found to be somewhat deficient relative to properties which have been attained, for example, by boron filaments. However, these properties can probably be improved in further development of the process by which the composite is made, because local waviness of the layers appears to account for the deficiencies.

The most important attribute of this form of composite material is that it is bidirectional, in contrast to filaments, which are unidirectional. Because of this, the weight of a film composite material which provides isotropic inplane stiffness, is about 60% of that of an equivalent filament-reinforced composite to provide the same stiffness. Structural efficiency analyses performed in this investigation showed that the potential weight savings offered by this bidirectional attribute can be significant for applications such as facings for sandwich cylinders and plates subjected to inplane compression, where biaxial stiffness benefits structural stability. These analyses also establish the proper proportions between the boron and supporting film to achieve minimum weight where elastic structural stability governs the composites'

design. It has been shown that for some applications the theoretically best proportions can be other than solid boron since the polyimide (or other supporting film) is less dense than boron. Generally optimum or efficient proportions call for less polyimide than was present in the film used in this investigation. It is therefore apparent that layered film composites offer significant gains in structural efficiency. This material also appears to be inherently well suited for fabricating developable shapes which may lead to economic advantages in addition to weight savings.

FABRICATION OF TUBULAR TEST SPECIMENS

The polyimide layers in the composite film investigated here are manufactured by E. I. DuPont de Nemours Co., Inc. under the trade name "Kapton" (Ref. 1). Kapton is synthesized by a polycondensation reaction between an aromatic tetrabasic acid and an aromatic amine. The boron layers are vacuum deposited on one side of the polyimide film by National Research Corporation.

Three tubular specimens were fabricated from boron-polyimide film by the method shown schematically in Figure 1. The wall thickness of the specimens consisted of five layers of the film plus an epoxy adhesive used to bond the layers together. After applying the adhesive to the film and wrapping it around a mandrel as indicated in Figure 1, a polyvinyl acetate tape was spirally wrapped over the specimens to press excessive adhesive from between the layers. The specimens were then oven cured at 100°C for six hours. Two of the specimens so fabricated had fairly uniform thicknesses, 43 percent of which was the adhesive. The film used in the third specimen became wrinkled and contained an excessive amount of adhesive (approximately 67 percent). Dimensions and composite densities of the specimens are summarized in Table I.

TABLE I - DIMENSIONS AND DENSITIES OF SPECIMENS

Specimen No.	Length (in.)	Average Diameter (in.)	Average Thick. (in x 10^3)	Boron Volume (%)	PI* Volume (%)	Epoxy Adhes (%)	Comp. Density (lb/in^3)
1	6.14	0.516	6.40	12.5	43.0	44.5	0.0527
2	8.43	0.520	10.71	7.5	25.8	66.7	0.0489
3	8.25	0.330	6.16	13.0	44.6	42.4	0.0529

*PI - Polyimide

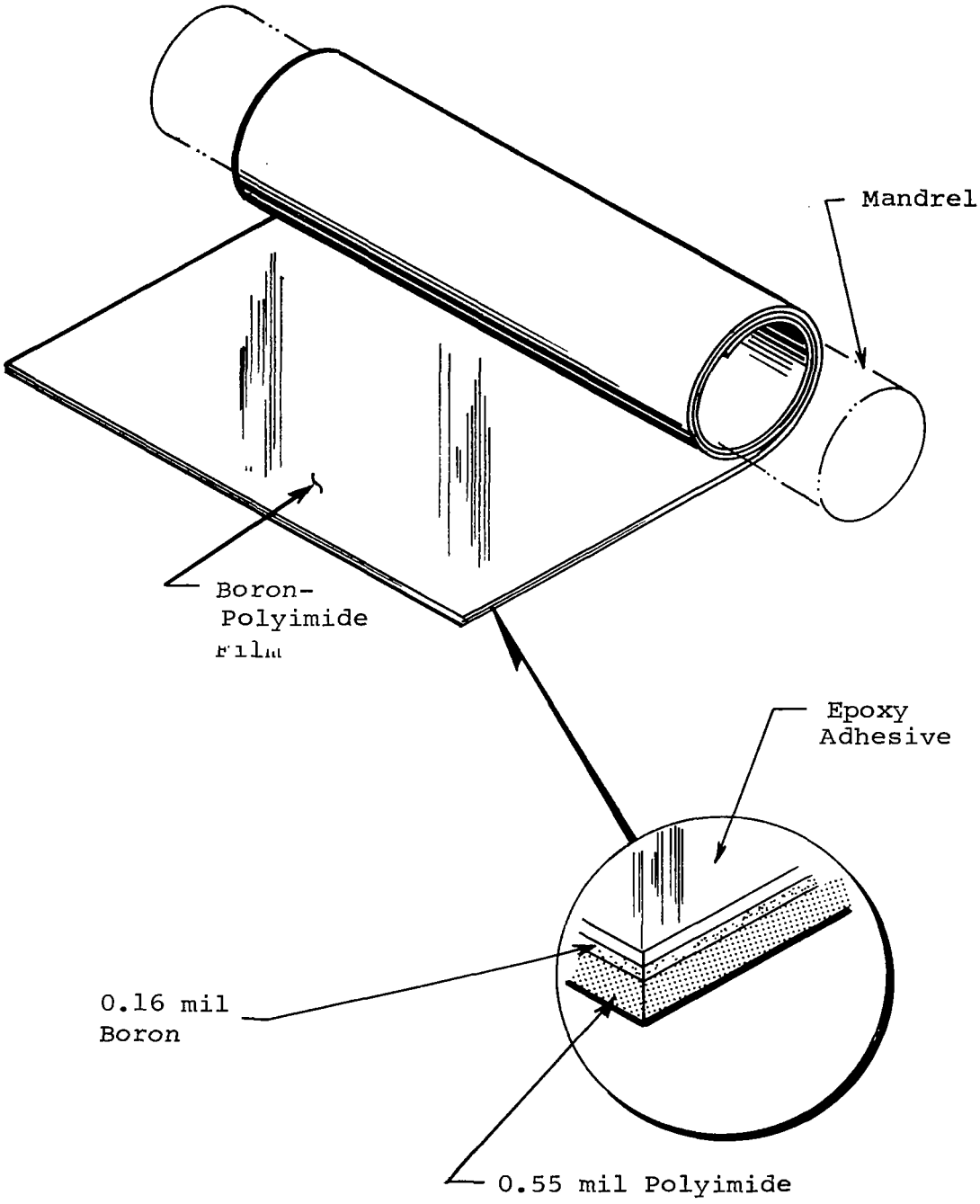

Figure 1 Schematic of Method Used to Fabricate Boron-Polyimide Tubular Test Specimens

The average thicknesses, volume percentages, and composite densities listed in Table I were calculated using the total weights and overall dimensions of the specimens, the average thicknesses of their boron and polyimide layers (as measured from photomicrographs of the specimens) and the nominal densities of the constituents listed in Table II.

TABLE II - DIMENSIONS AND PROPERTIES OF CONSTITUENTS

Constituent	Density (lb/in^3)	Single Layer Thickness (in. x 10^3)	Young's Modulus (psi x 10^{-6})
Boron	0.090	0.16	60.0
Polyimide	0.051	0.55	0.5
Epoxy	0.043	(see Table I)	0.5

Photomicrographs of sections of Specimen 1 are shown in Figures 2(a) through 2(d). The thicknesses of the boron and polyimide layers given in Table II are average values of filar micrometer measurements of the sections shown in Figure 2. It may be seen from these sections, particularly Figure 2(c), that the thickness of the boron and polyimide layers is quite uniform. Some breaks in the boron are observed in the longitudinal sections, but they are not extensive. However, Figure 2(d), the circumferential section, shows that very extensive cracks exist in that direction, which perhaps created voids in the composite. By comparing the two longitudinal sections of Figures 2(a) and 2(b), it is observed that the epoxy adhesive layers are not of uniform thickness, and waviness of the layers exists in some sections of the specimen but not in others.

TEST PROCEDURES AND RESULTS

The test specimens, with their steel end fittings, are shown in Figure 3. Each of the three specimens was subjected to axial compression tests and then to flexural tests.

Axial compression tests were performed with the hydraulic testing apparatus shown in Figure 4. The loads were applied through spherical steel balls which were placed between the specimen seats in the specimen end fittings and the loading heads. Thus, eccentricity of loading was minimized. Both head travel and

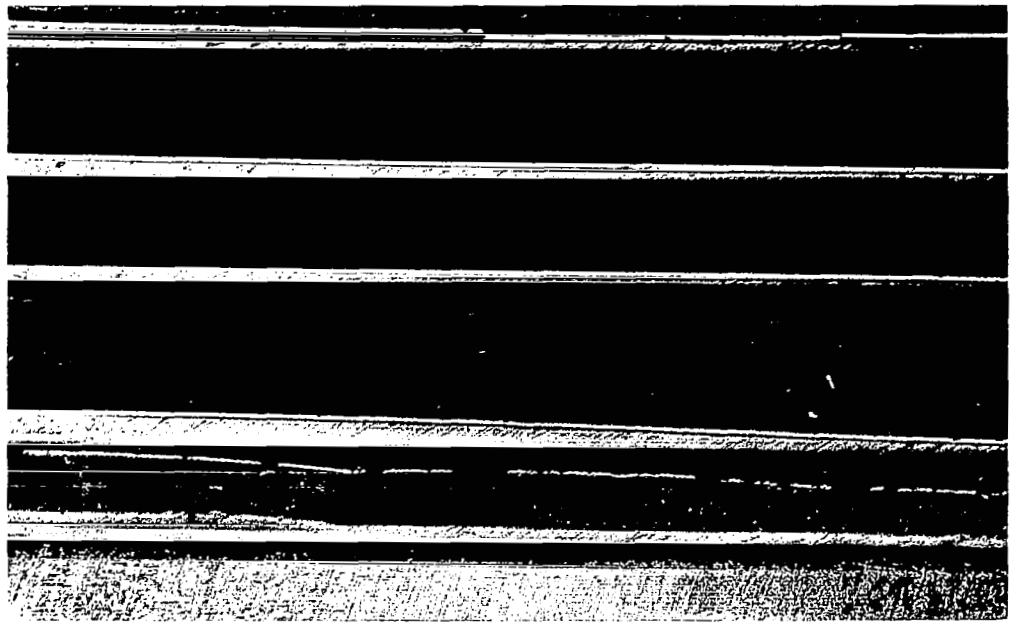

Figure 2(a). Longitudinal Section of Composite, Specimen 1, Position 1

Figure 2(b). Longitudinal Section of Composite Specimen 1, Position 2

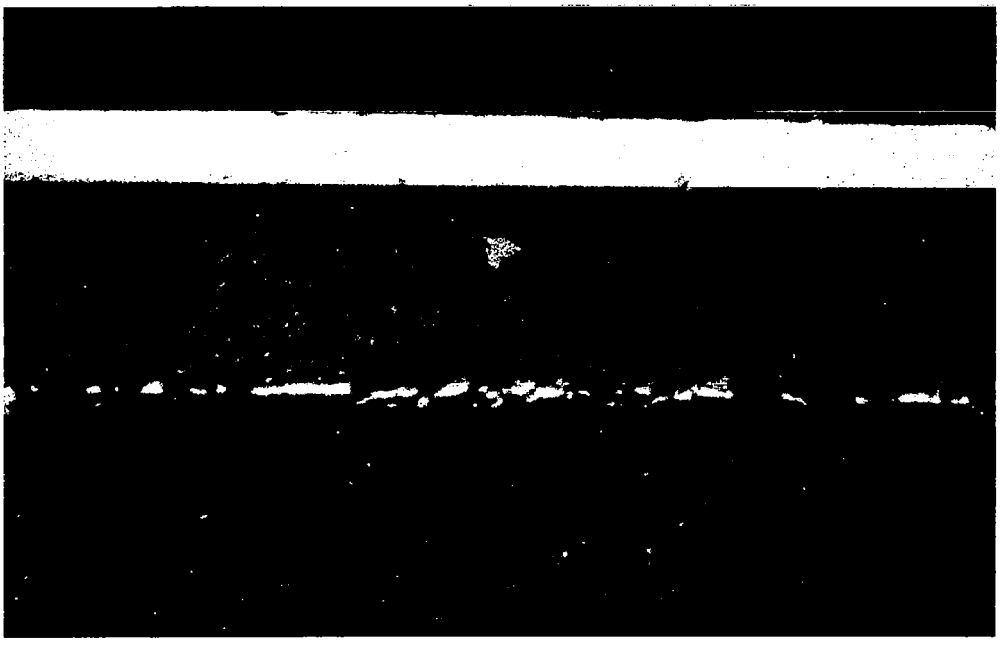

Figure 2(c) Enlargement of Longitudinal Section

Figure 2(d) Circumferential Section of Composite

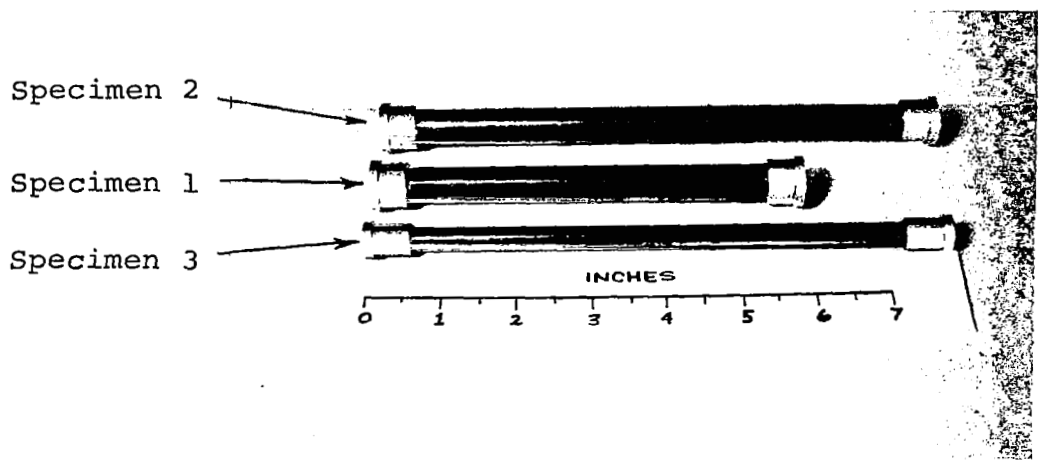

Figure 3. Finished Test Specimens with End Fittings

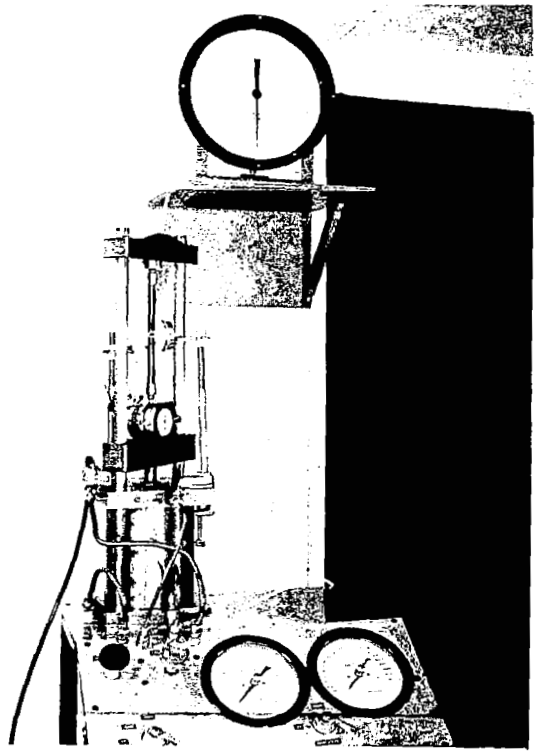

Figure 4. Apparatus and Specimen Ready for Axial Compression Test

lateral deflection of the specimen were monitored during loading. The specimens were loaded until they failed, as shown in Figure 5.

Table III shows the failure load of each specimen and the types of failure.

TABLE III - AXIAL COMPRESSION TEST RESULTS

Specimen Number	Failure Load lbs.	Type of Failure
1	175	Local buckling at one-third length
2	134	Wrinkling near end fitting
3	111	Lateral deflection of specimen followed by tensile fracture

After the axial compression tests were performed, the undamaged portions of the specimens were tested in flexure as shown in Figure 6. The objective of this set of tests was to determine the moduli of elasticity of the specimens as exhibited in flexure, for comparison with their moduli as exhibited in the axial compression tests. The composite moduli of elasticity derived from the results of both sets of tests are given in Table IV. These moduli are based on the load-deformation measurements and the average thicknesses listed in Table I. The values of predicted moduli that also appear in Table IV were calculated by using in the rule of mixtures, the volume percentages of the constituents given in Table I and the constituent moduli given in Table II.

TABLE IV - MEASURED AND PREDICTED VALUES OF COMPOSITE MODULI

Specimen Number	Composite Modulus (psi x 10^{-6})		
	Axial Comp. Tests	Flexural Tests	Predicted Moduli
1	5.57	6.61	7.95
2	2.39	4.30	4.93
3	7.40	6.09	8.22

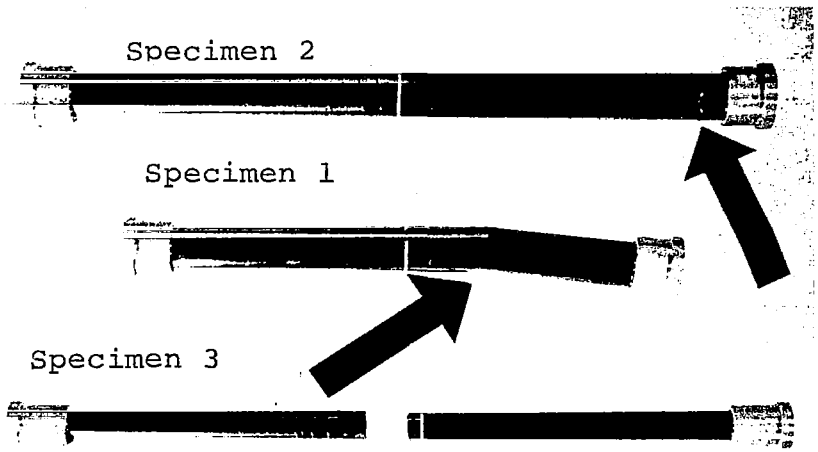

Figure 5. Test Specimens After Failure Due to Axial Compression

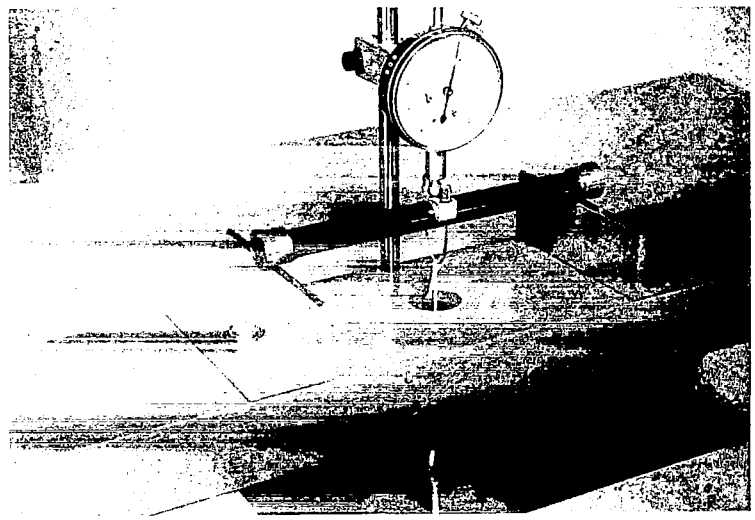

Figure 6. Apparatus and Specimen Ready for Flexure Test

The specimens were not loaded to failure in the flexure tests; however, Specimens No. 1 and 3 were flexed until a slight amount of nonlinearity began to develop in their load-deflection characteristics. Maximum composite stresses developed in the flexure tests are listed in Table V, along with the maximum stresses in the axial load tests. Stresses shown for the flexure tests are based on the applied moments and the section dimensions of Table I.

TABLE V - MAXIMUM COMPOSITE STRESSES

Specimen Number	Maximum Stress (ksi)	
	Flexure Tests	Compression Tests
1	13.6	17.1
2	----	7.8
3	14.3	17.7

DISCUSSION AND ANALYSIS OF RESULTS

The average modulus of elasticity exhibited by Specimens 1 and 3 was 6.42×10^6 psi, and their average density was 0.528 pci. The performance of Specimen 2 is not included in this discussion because the specimen was clearly defective. The predicted values of the composite moduli for Specimens 1 and 3, given in Table IV, indicate that this average value of the measured modulus was about 80 percent of the value it would have been if the boron had developed a modulus of 60×10^6 psi. In fact, the average effective modulus of the boron in Specimens 1 and 3 was 47.3×10^6 psi based on the test results shown in Table IV and averages of the volume percentages of the constituents given in Table I.

The average value of the composite compression strength developed by Specimens 1 and 3 was about 17.4 ksi. The strain at failure was then approximately 2.16×10^{-3}. The corresponding failure stress in the boron, using a modulus of 47.3×10^6 psi was 102 000 psi. The maximum tensile stress to which the specimens were subjected in the flexure tests was approximately 82 000 psi. Those tests were terminated at the onset of nonlinearity which was probably the result of instability on the compressive sides.

A possible cause of the apparent deficiency in the modulus of the boron layers is that the density and physical state of deposited boron may be different from that of filaments for which moduli of approximately 60 x 10^6 psi have been developed. Additional crystallographic examination of the boron layers formed by vacuum deposition on relatively cool surfaces may resolve this question.

It also appears possible that waviness of the thin boron layers could account for this deficiency. The effective modulus of composites with initially wavy layers of boron imbedded between and bonded to layers of another material is analyzed in the Appendix. The analyses are for the two different types of waviness shown in Figure 7. One case in Figure 7 shows the waviness of adjacent layers to be symmetric about planes midway between them. The amplitudes of the initial imperfections grow but remain symmetric as inplane loads are applied. The intermediate, softer layers are strained in their thickness direction to accommodate the imperfection growth. These lateral displacements of the boron layers result in additional inplane compliance and effectively lower the composite modulus.

For the second case depicted in Figure 7, the initial waviness of adjacent layers is antisymmetric about midplanes; waves in adjacent layers are inphase. In this case, the intermediate layers undergo shear deformation as the wave amplitudes are increased by end loading.

The apparent modulus for the symmetric case is derived in the Appendix, Equation (A21);

$$\frac{\overline{E}_B}{E_B} = \left[1 + \frac{6\,(1 - \nu_B^2)\,\left(\frac{A}{t_B}\right)^2}{1 + 3\left(\frac{2}{\pi}\right)^4 \frac{(1 - \nu_B^2)}{(1 - \nu_M^2)}\,\frac{E_M}{E_B}\,\frac{t_B}{t_M}\,\left(\frac{\lambda}{t_B}\right)^4} \right]^{-1} \qquad (1)$$

The symbols are defined in the List of Symbols.

For the antisymmetric case, the apparent modulus is obtained from Equation (A36) as

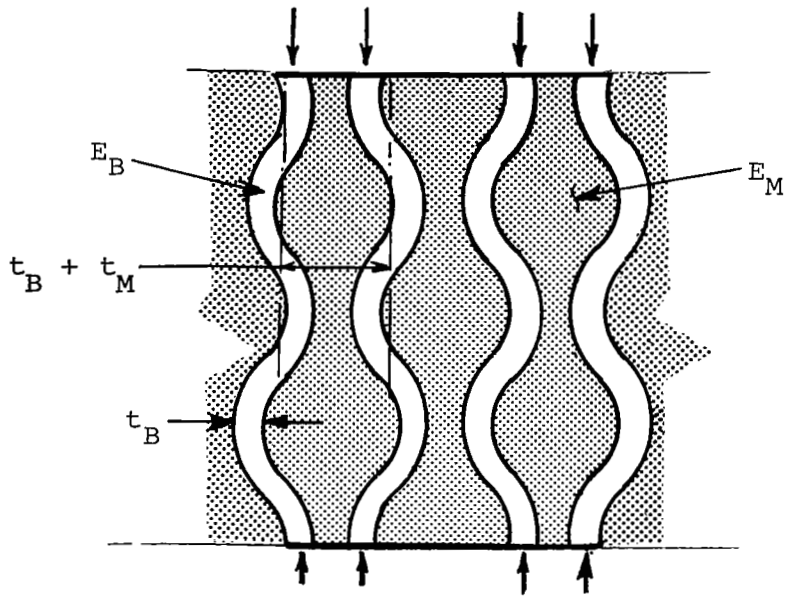

a. Symmetric Imperfections

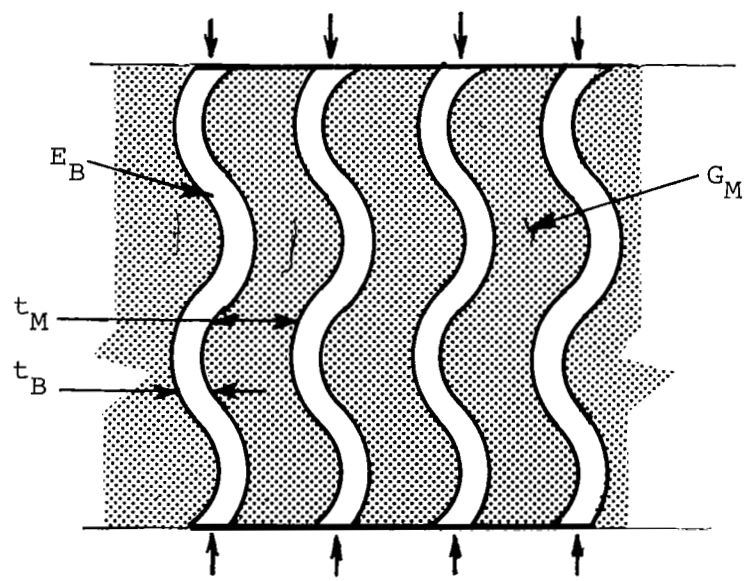

b.

Figure 7. Geometry of Initially Imperfect Composite

$$\frac{\overline{E}_B}{E_B} = \left[1 + \frac{\frac{\pi^2}{2} \frac{E_B}{G_M} \frac{t_B}{t_M} \left(\frac{A}{t_B}\right)^2}{\left(\frac{\lambda}{t_B}\right)^2 \left(1 + \frac{t_B}{t_M}\right)^2 \frac{\pi^2}{12\,(1 - \nu_B^2)} \frac{E_B}{G_M} \frac{t_B}{t_M}} \right]^{-1} \qquad (2)$$

In Reference 2, Schuerch shows that the critical composite stress for buckling of initially straight layers in the symmetric mode is

$$\sigma_{C_{CR}}\Big|_{SYM} = \frac{2}{\sqrt{3}} E_C \sqrt{\frac{E_M}{E_B} \frac{t_B}{t_M} (1-\nu_B^2)^{-1} (1-\nu_M^2)^{-1}} \qquad (3)$$

The solution obtained in the Appendix for the antisymmetric mode differs from that of Reference 2 by the presence of the final factor on the right hand side of the following equation:

$$\sigma_{C_{CR}}\Big|_{ANTI} = G_M \left(1 + \frac{t_B}{t_M}\right) \left(1 + \frac{E_M}{E_B} \frac{t_M}{t_B}\right) \qquad (4)$$

The average critical stresses for Specimens 1 and 3 are

$$\sigma_{C_{CR}}\Big|_{SYM} = 354 \times 10^3 \text{ psi}$$

$$\sigma_{C_{CR}}\Big|_{ANTI} = 227 \times 10^3 \text{ psi}$$

when the following nominal properties of Specimens 1 and 3 are used:

$t_B = 0.16$ mil $\qquad E_M = 0.50 \times 10^6$ psi $\qquad \nu_M = 0.33$

$t_M = 1.10$ mils $\qquad E_B = 60 \times 10^6$ psi $\qquad$ and $G_M = \frac{3}{8} E_M$

$E_C = 8.08 \times 10^6$ psi $\qquad \nu_B = 0.25$

Since these values of critical stresses are much greater than the 17 ksi stresses applied in the tests, the effects of loading parameters, α_w and α_s, (see Appendix) have been neglected in Equations (1) and (2) for purposes of examining the effects of waviness on the apparent modulus at low stress levels. Accordingly, Figures 8 and 9 are graphs of Equations (1) and (2) showing values of $\overline{E}_B/E_B$ for the symmetric and antisymmetric cases for the nominal properties of Specimens 1 and 3. These graphs of $\overline{E}_B/E_B$ versus the imperfection amplitude parameter, A/t_B, and wavelength parameter, λ/t_B, show that the observed deficiency in the boron modulus ($\overline{E}_B/E_B = 0.79$ for $E_B = 60 \times 10^6$ psi) could have resulted from a wide range of combinations of the two imperfection parameters.

Referring now to Figure 2, the photomicrograph of one of the longitudinal sections shows no initial waviness large enough to cause significant reduction in the boron's effective modulus. However, the other longitudinal section contains initial imperfections, predominately antisymmetric, which would have reduced the effective modulus to much less than that measured if it existed throughout the specimen. For example, the second layer from the top in Figure 2(b) has an A/t_B greater than 5 with λ/t_B equal to about 80. A general waviness of that extent would cause severe reduction in effective modulus. It must therefore be concluded that if the parent modulus of the deposited boron is indeed 60×10^6 psi, then the average waviness of the boron layers in the specimens was small - somewhere between the two extremes shown in Figures 2(a) and (b) - but sufficiently severe to cause the observed reduction in effective modulus.

Consider next the ultimate compression strengths developed by the specimens tested. The tensile failure of Specimen 3 during its axial load test was clearly the result of excessive bending that developed when it became unstable. Its predicted Euler load is 74.6 lbs., based on an effective length of 8.97 in. (distance between centers of load spheres) and an elastic modulus of 7.40×10^6 psi. Friction in the spherical seats may account for the failure load exceeding the Euler load.

The failure regions of Specimens 1 and 2 showed delamination when inspected after the axial load tests. In fact, the failure region of Specimen 2 consisted only of delaminations in the form of outward wrinkles. The failure region of Specimen 1 was an inward buckle with delamination in that area. Both of these specimens failed at stresses well below those predicted for either local

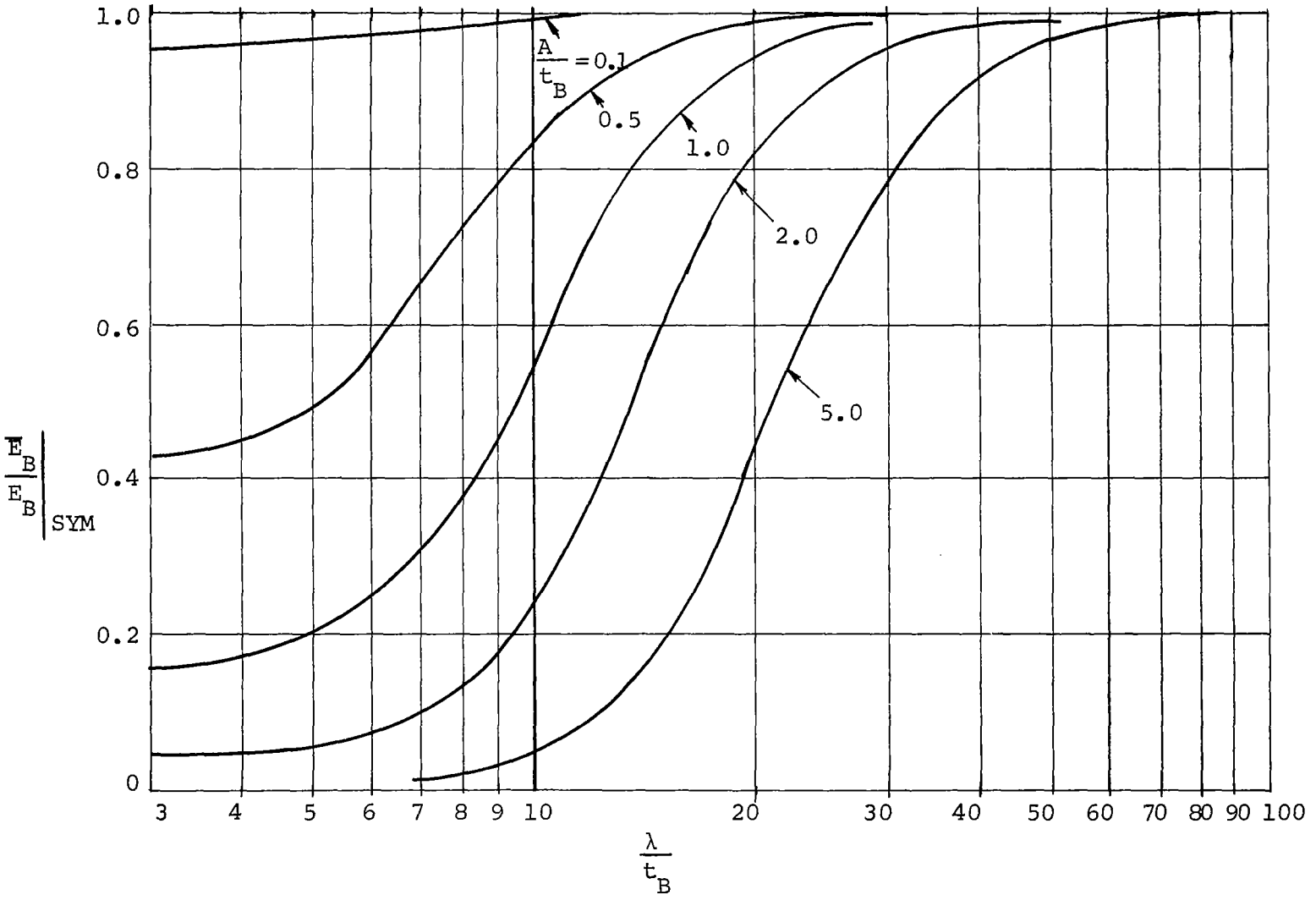

Figure 8. Effects of Symmetric Initial Imperfections on Effective Modulus of Boron Layers

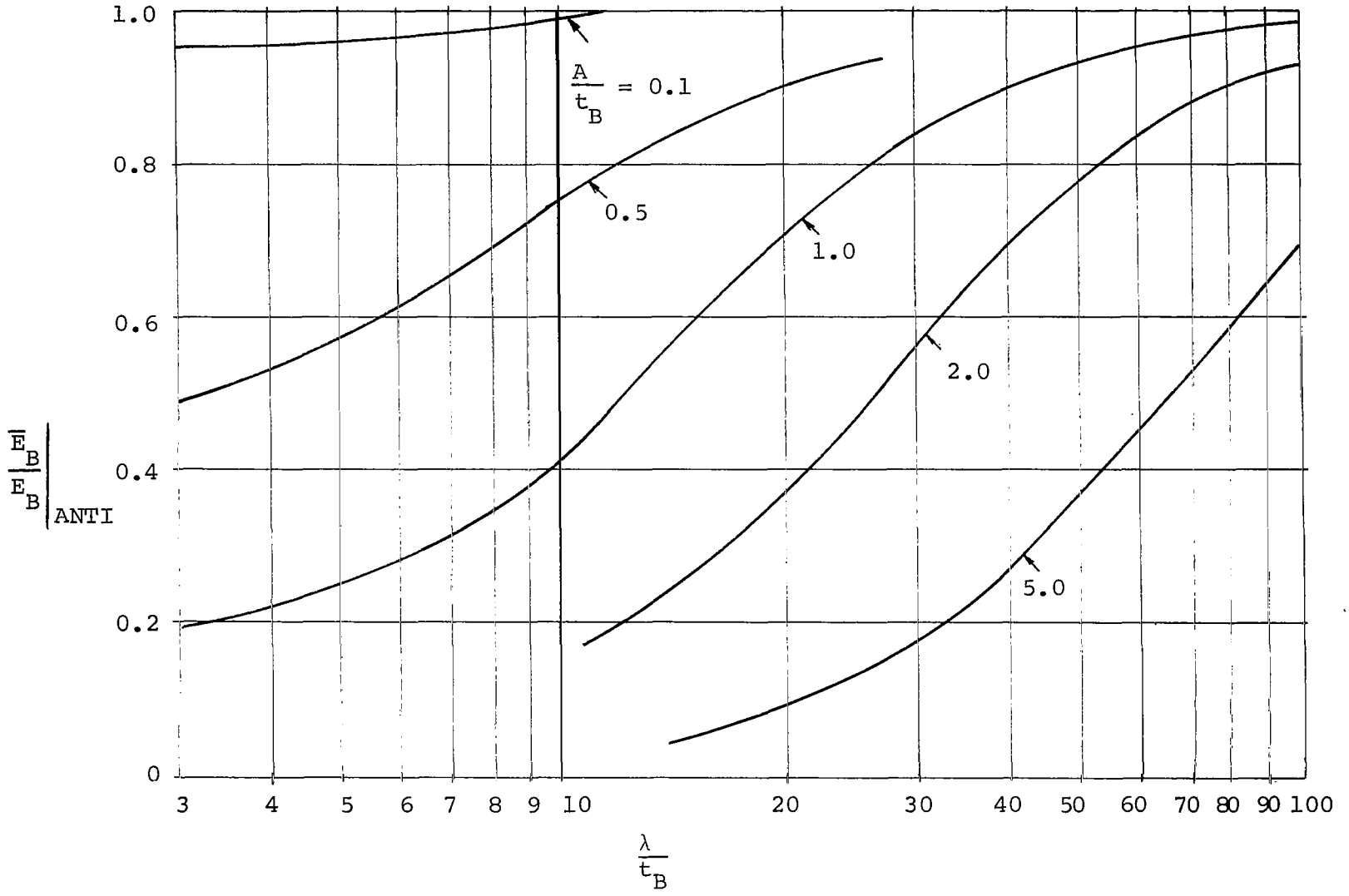

Figure 9. Effects of Antisymmetric Initial Imperfections on Effective Modulus of Boron Layers.

shell buckling, Euler buckling or the internal modes of failure as predicted by Equations (3) and (4). It is therefore suspected that delamination was the cause of failure for both Specimens 1 and 2.

Initial waviness of the boron layers could have caused direct or shear stresses on the interfaces between the boron and epoxy layers, which could then result in delamination. The maximum interface tension stress that symmetric initial waviness would cause is given in the Appendix by Equation (A25), and the maximum shearing stress caused by antisymmetric waviness is given by Equation (A40). Figure 10 shows the values of the tension and shear stresses for the approximate load and properties of Specimen 1. In Figure 10, the maximum tension and shear stresses are shown to vary significantly with the waviness parameters, A/t_B and λ/t_B. They are greatest, for any given value of A/t_B, when λ/t_B is in the range of 6 to 7. For a given value of λ/t_B, the stress increases with increased values of A/t_B.

The interface strength of the present layered composites is not known; however, strengths in the vicinity of 1 to 10 ksi would appear reasonable. Figure 10 shows that the previously cited waviness from Figure 2(b), $A/t_B > 5$ and $\lambda/t_B = 80$, would cause shear stresses of 3.5 ksi - perhaps enough to result in delamination.

Initial imperfections in the vicinity of the failure regions might have been large enough to produce shear or tension stresses on the interfaces and cause delamination. Or, unbonded areas in the specimens may have existed which propagated under load to cause their general failure. Further investigation of these possibilities was not performed in this study, but would be appropriate in future development of this type of composite.

STRUCTURAL EFFICIENCY POTENTIALS

This assessment of potential structural efficiencies for boron-polyimide composites is limited to applications in which elastic structural stability governs design. These composites have isotropic extensional and flexural stiffness in their plane. Therefore, results of structural-efficiency studies that have been made for both monocoque and built-up structures using homogeneous materials, can be used in this assessment.

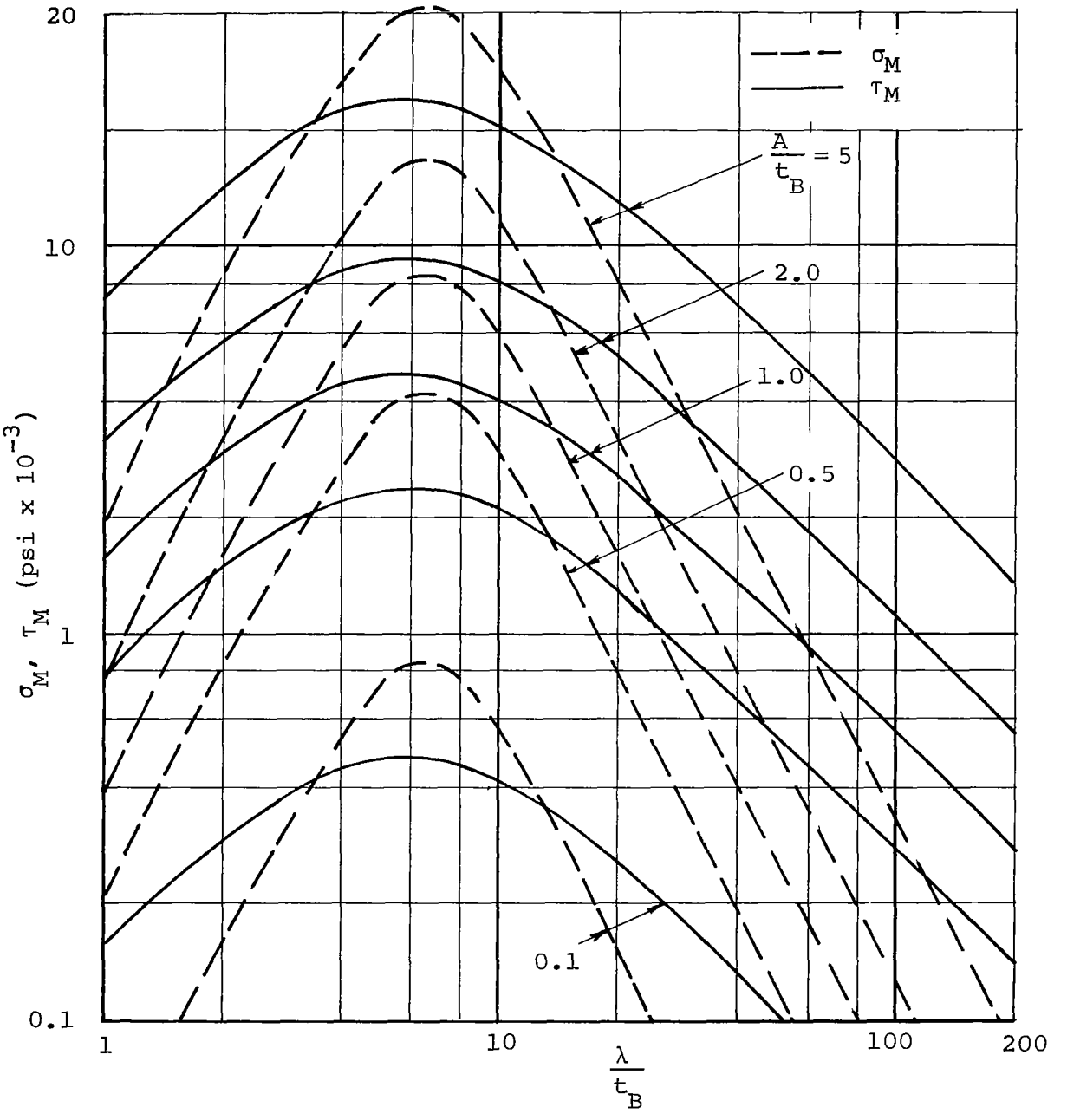

Figure 10. Maximum Values of Direct and Shearing Stresses versus Waviness Parameters A/t_B and λ/t_B

The general form of the structural efficiency equation for columns, wide columns, compression panels, cylinders under axial compression or hydrostatic pressure, or for box beams in bending is (see Refs. 3, 4, and 5, for examples):

$$W = \frac{d}{E^{1/n}} \; F \; I^{1/n} \tag{5}$$

where W is the structural weight per unit area, per unit length or is referred to some other characteristic dimension of the structure

d is the structural material's density

E is its Young's modulus

F is a nondimensional quantity related to the geometric proportions of the structure and its stiffening. This quantity is minimized for a structure of optimum proportions

I is a structural loading index which expresses the loading intensity

and n is a nondimensional exponent whose value is typically between 1.67 and 3, see Ref. 5. Its value depends on the type of structural function (e.g., column or cylinder) and the type of detailed construction (e.g., monocoque, stiffened or sandwich).

The density and Young's modulus of boron-polyimide composites depend on their proportions in the composite as calculated by the rule of mixtures;

$$d_C = \frac{d_B}{1 + \frac{t_M}{t_B}} \left(1 + \frac{d_M}{d_B} \; \frac{t_M}{t_B} \right) \tag{6}$$

$$E_C = \frac{KE_B}{1 + \frac{t_M}{t_B}} \left(1 + \frac{1}{K} \; \frac{E_M}{E_B} \; \frac{t_M}{t_B} \right) \tag{7}$$

The subscript B refers to boron and the subscript M refers to the total matrix layer of polyimide film and epoxy adhesive between adjacent boron layers. An average density, 0.045 pci, and an average modulus of 0.5 x 10^6 psi are used for the matrix layers in the present assessment. The factor K in Equation (7) is used to express the fractional part of E_B which is realized - that is,

$$K = \frac{\overline{E}_B}{E_B} \tag{8}$$

The ratio of the weight of a boron-polyimide-epoxy composite structure to that of a reference structure of solid boron, each designed to perform the same structural function (specified by I) with geometric proportions of the same structural efficiency (characterized by F), is found by Equation (5);

$$\frac{W_C}{W_B} = \frac{d_C}{d_B}\left(\frac{E_B}{E_C}\right)^{1/n} \tag{9}$$

By substituting Equations (6) and (7) in (9) and using subscripted r's to designate the ratios of weights, densities, thicknesses and moduli (see list of symbols), the following formula for the weight ratio is obtained:

$$r_W = \frac{1}{K^{1/n}} \frac{(1 + r_D\, r_t)}{(1 + r_t)^{\frac{n-1}{n}} (1 + r_E\, r_t)^{1/n}} \tag{10}$$

A graph of the weight ratio, r_W, versus the mixture ratio, r_t, is given by the solid lines in Figure 11 for the ideal case when K = 1, r_D = 0.5, and r_E = 0.00833 for three typical values of n. When K = 1, the boron layers develop their full potential modulus. The dashed lines in Figure 11 show the weight ratio versus mixture ratio for K = 0.80, r_D = 0.5, and r_E = 0.0104. These approximate values of K, r_D, and r_E have been realized for the composites in this program.

The average value of r_t for Specimens 1 and 3 was 6.85. Figure 11 shows that, depending on the value of n for a particular application, the present composite and mixture ratio could be used

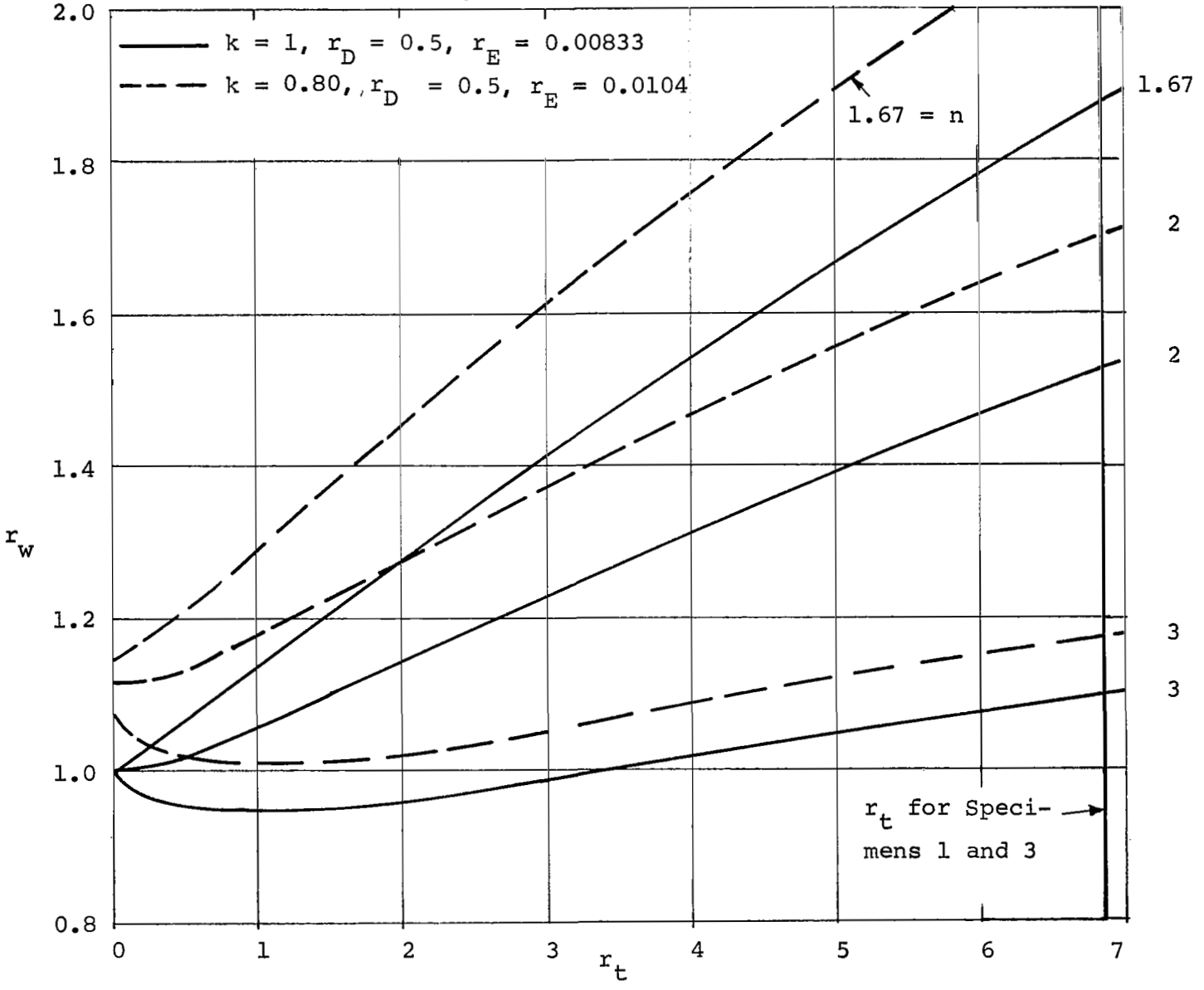

Figure 11. Ratio of Boron-Polyimide Composite Structural Weights to Those of Solid Boron to Perform the Same Function

to produce a structure weighing from 1.18 to 2.1 times that of a solid boron structure with $E_B = 60 \times 10^6$. The difference between dashed and solid lines in Figure 10 shows the potential gains from developing the composite film and manufacturing process toward the attainment of $K = 1$. The differences in r_W between $r_t = 6.85$ and lower values of r_t are the potential gains from developing films and manufacturing processes whereby more effective mixture ratios could be produced.

It is also noted from Equation (10) and Figure 11 that r_W is minimized at values of r_t other than zero for certain combinations of n, r_E, and r_D. Specifically,

$$r_t\Big|_{opt} = \frac{n(1-r_D) - (1-r_E)}{r_D\,(1-r_E) - n\,r_E\,(1-r_D)} \tag{11}$$

provided r_t is not negative. For these optimum values of the mixture ratio,

$$r_W\Big|_{min} = \frac{n\left(\frac{r_D - r_E}{n-1}\right)^{\frac{n-1}{n}}}{(1-r_E)\quad(1-r_D)} \tag{12}$$

To demonstrate further the potential efficiency of layered boron-polyimide composites, consider the ratio of their weights to those of beryllium, magnesium, and aluminum, each designed to perform the same structural function. Table VI gives a set of these ratios for the case $n = 2$ and for three different values of r_t.

TABLE VI - WEIGHT RATIOS FOR n = 2

r_t	$\frac{W_c}{W_{Be}}$	$\frac{W_c}{W_{Mg}}$	$\frac{W_c}{W_{Al}}$
6.85	2.03	0.726	0.626
3	1.63	0.625	0.505
1	1.405	0.540	0.435

These ratios were determined from an expression similar to Equation (9) except that the above metal properties were substituted for those of the hypothetical solid boron. The composite properties used in evaluating the ratios were the average values for Specimens 1 and 3. The first value of r_t in Table VI was the average for the two specimens, but the other two values of r_t are hypothetical. The weight ratios listed in Table VI clearly demonstrate the advantage of this type of layered composite over magnesium and aluminum; beryllium, however, is still theoretically the lighter structure.

As a final and very significant demonstration of the structural efficiency potentials of boron-polyimide film composites, consider the basic advantage that a film composite derives from its biaxial stiffness. Reference 6 shows that for axially compressed cylinders of sandwich construction with the facings made of filament composites, the filament orientations should be so dispersed that the resulting composite facings have isotropic stiffness in their plane. This type of dispersion will produce a minimum-weight sandwich cylinder for designs governed by elastic stability requirements.

Now, to achieve this inplane isotropy with filaments, the value of K is effectively 0.375. For example, isotropy is achieved by distributing one third of the filaments in each of three directions 0 and $\pm 60°$ from the loading direction. This value of K is based on all filaments developing their full potential modulus in their axial directions. Figure 12 is a comparison of the weight ratio of this type of boron-filament construction with the boron-laminate type of construction. The comparisons are based on Equation (10) with $n = 2$ and $r_D = 0.5$. The weight in each case is normalized with respect to the weight of sandwich structure with hypothetical, solid-boron facings to perform the same structural function. The comparison made in Figure 12 clearly demonstrates the advantage of the present boron-polyimide film due to its inherent biaxial stiffness. The differences between the weights for filament and film composites shown in Figure 12 would be even greater if the full potential for the film's modulus, $K = 1$, were used in the comparison.

In cases where only unidirectional properties affect stability, the theoretical potential for film composites is the same as that for filament composites when each has the same mixture ratio.

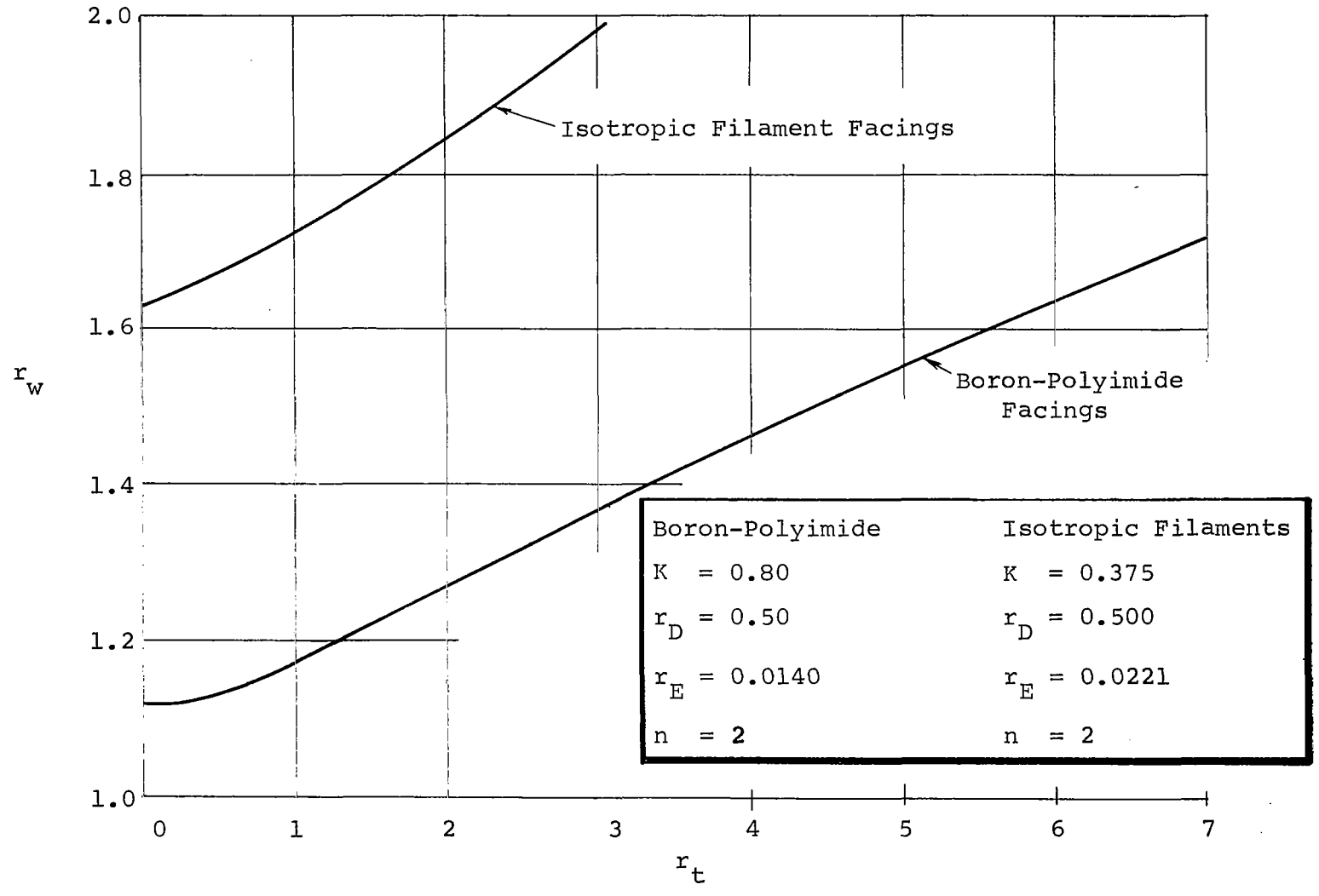

Figure 12. Comparison of Structural Weights for Filament and Film Reinforced Sandwich Facings for Axially Compressed Composites

CONCLUSIONS AND RECOMMENDATIONS

1. This study has demonstrated that boron-polyimide composites are practical to fabricate and have excellent potential for high structural efficiency when elastic stability requirements govern their design.

2. The effective Young's modulus developed by the boron layers (47×10^6 psi) appeared to be somewhat deficient. This may be attributable either to deleterious effects of initial waviness in the boron layers, or the basic properties of the deposited boron may be deficient due to its crystallography.

3. The specimens also showed a rather low compressive strength which appeared to be the result of initial waviness and subsequent delamination under load. If initial waviness proves to have been the cause of low compressive strength, it can probably be remedied by development of better fabrication processes.

4. Higher levels of structural efficiency than have been demonstrated by the specimens of this program can be attained by increasing the proportions of boron present.

5. Other layered composites of low-density matrices and high-modulus structural materials should be evaluated for their weight-saving potential and fabricability.

REFERENCES

1. DuPont Kapton* Polyimide Film, Summary of Properties, Bulletin H-1A, E. I. DuPont de Nemours & Co., Inc.

2. Schuerch, H., "Prediction of Compressive Strength in Uniaxial Boron Fiber - Metal Matrix Composite Materials", AIAA Journal, Volume 4, No. 1, January 1966, pp. 102-106.

3. Shanley, F. R., "Weight-Strength Analysis of Aircraft Structures", McGraw-Hill Book Co., New York, 1952.

4. Gerard, G., "Minimum Weight Analysis of Compression Structures", N. Y. University Press, New York, 1956.

5. Crawford, R. F., and Burns, A. B., "Minimum Weight Potentials for Stiffened Plates and Shells", AIAA Journal, Volume I, No. 4, April 1963, pp. 879-886.

6. Dow, N. F., and Rosen, B. W., "Structural Efficiency of Orthotropic Cylindrical Shells Subjected to Axial Compression", AIAA Journal, Volume 4, No. 3, March 1966, pp. 481-486.

7. Timoshenko, S., "Theory of Elastic Stability", McGraw-Hill Book Co., New York, 1963, p. 30.

*DuPont Registered Trademark

APPENDIX

DERIVATION OF EFFECTIVE MODULUS OF BORON STRATA

Schematics of the layered boron-polimide-epoxy composites in their symmetric and antisymmetric modes of initial imperfection are shown in Figure 7a and 7b. In each case, it is assumed that the polyimide-epoxy layers are one homogeneous, constant thickness matrix, t_M. The boron layer is also of constant thickness t_B. The Young's modulus of the boron is E_B and that of the matrix is E_M. The shearing modulus of the matrix is G_M. In each case a plane strain distribution and an initial imperfection, y_o, given by the following equation are assumed to exist:

$$y_o = A \sin \frac{\pi x}{\lambda} \tag{A1}$$

Also, in each case the layers are assumed to deflect by the amount y_1 under application of the end load:

$$y_1 = B \sin \frac{\pi x}{\lambda} \tag{A2}$$

In the symmetric case, the initial imperfections of the adjacent boron layers are assumed to be π radians out of phase and to retain that phase angle under end load. Similarly, in the antisymmetric case deflections of the adjacent layers are assumed to be initially inphase and remain so.

Symmetric Case:

It is assumed that effects of shearing in the matrix can be neglected because wavelengths of initial imperfections will be much greater than the matrix thickness. The matrix then becomes a Winkler foundation of stiffness $4E_M/[t_M (1-\nu_M^2)]$ per unit width and length of the boron layers. This stiffness resists amplification of the initial imperfection mode. The differential equation of equilibrium is then

$$M_B'' + N_B (y_o'' + y_1'') = k_M y_1 \tag{A3}$$

where

$$M_B = D_B y_1'' \tag{A4}$$

and primes denote differentiation with respect to x.

$$D_B = \frac{E_B t_B^3}{12(1-\nu_B^2)} \tag{A5}$$

$$N_B = \sigma_B t_B \tag{A6}$$

$$k_M = \frac{4E_M}{t_M(1-\nu_M^2)} \tag{A7}$$

By substituting M_B, y_o and y_1 as given above into Equation (A3), the following relationship between amplitudes A and B is obtained

$$\frac{B}{A} = \frac{\frac{N_B}{D_B}\left(\frac{\lambda}{\pi}\right)^2}{1 - \frac{N_B}{D_B}\left(\frac{\lambda}{\pi}\right)^2 + \frac{k_M}{D_B}\left(\frac{\lambda}{\pi}\right)^4} \tag{A8}$$

The critical value of N_B is that which causes B to increase indefinitely;

$$N_B = D_B\left(\frac{\pi}{\lambda}\right)^2 + k_M\left(\frac{\lambda}{\pi}\right)^2 \tag{A9}$$

Minimization of N_B with respect to λ gives

$$\lambda_w = \pi\left(\frac{D_B}{k_M}\right)^{\frac{1}{4}} \tag{A10}$$

for which

$$N_{B_{CR}} = 2\sqrt{k_M D_B} \tag{A11}$$

This critical buckling load is the same as that given in Reference 2 and is referred to here as the wrinkling mode; hence the w subscript on λ above. The following definition is used for the end load ratio:

$$\alpha_w = \frac{N_B}{N_{B_{CR}}} = \frac{N_C}{N_{C_{CR}}} = \frac{\sigma_C}{\sigma_{C_{CR}}} \tag{A12}$$

By combining Equations (A8), (A10), (A11), and (A12), the amplitude B is expressed in the following form

$$\frac{B}{A} = \frac{\alpha_w \left(\frac{\lambda}{\lambda_w}\right)^2}{\frac{1}{2}\left[1 + \left(\frac{\lambda}{\lambda_w}\right)^4\right] - \alpha_w \left(\frac{\lambda}{\lambda_w}\right)^2} \tag{A13}$$

Now, the increment of end shortening per wavelength that results from deflecting the layers from amplitude A to A + B is that for deflecting it from zero to A + B less than for deflecting it from zero to A;

$$\delta = \delta_{A+B} - \delta_B \tag{A14}$$

From Reference 7 it is readily seen that

$$\delta_A = \frac{\pi^2 A^2}{4\lambda} \tag{A15}$$

and

$$\delta_{B+A} = \frac{\pi^2}{4\lambda} (A + B)^2 \tag{A16}$$

Therefore,

$$\delta = \frac{\pi^2 A^2}{4\lambda} \frac{B}{A} \left(2 + \frac{B}{A}\right) \tag{A17}$$

By substituting Equation (A13) for B/A in this expression for δ,

$$\delta = \left(\frac{\pi A}{2}\right)^2 \frac{\alpha_w}{\lambda}\left(\frac{\lambda}{\lambda_w}\right)^2 \left\{ \frac{1 + \left(\frac{\lambda}{\lambda_w}\right)^2 - \alpha_w \left(\frac{\lambda}{\lambda_w}\right)^2}{\left[\frac{1}{2} + \frac{1}{2}\left(\frac{\lambda}{\lambda_w}\right)^4 - \alpha_w \left(\frac{\lambda}{\lambda_w}\right)^2\right]^2} \right\} \tag{A18}$$

The total displacement of the end of a boron layer is then that due to axial shortening plus δ. By defining $\overline{E}_B$ as an effective modulus that accounts for both these contributions, the following relations are obtained

$$\delta_T = \delta_{AXIAL} + \delta \tag{A19}$$

or

$$\frac{N_B \lambda}{t_B \overline{E}_B} = \frac{N_B \lambda}{t_B E_B} + \delta \tag{A20}$$

By combining Equations (A18), (A20), and the foregoing definitions, the ratio $\overline{E}_B/E_B$ is obtained as follows:

$$\frac{\overline{E}_B}{E_B} = \frac{1}{1 + \frac{3}{2}\left(\frac{A}{t_B}\right)^2 \left(1 - \nu_B^2\right) \left\{ \frac{1 + \left(\frac{\lambda}{\lambda_w}\right)^4 - \alpha_w \left(\frac{\lambda}{\lambda_w}\right)^2}{\left[\frac{1}{2} + \frac{1}{2}\left(\frac{\lambda}{\lambda_w}\right)^4 - \alpha_w \left(\frac{\lambda}{\lambda_w}\right)^2\right]^2} \right\}} \tag{A21}$$

From the above work, λ/λ_w can be expressed as

$$\frac{\lambda}{\lambda_w} = \frac{\lambda}{t_B} \frac{2}{\pi} \left[3 \frac{\left(1 - \nu_B^2\right)}{\left(1 - \nu_M^2\right)} \frac{E_M}{E_B} \frac{t_B}{t_M} \right]^{1/4} \tag{A22}$$

For a composite having properties equal to the averages of those for Specimens 1 and 3

$$\frac{\lambda}{\lambda_w} \cong 0.1542 \frac{\lambda}{t_B} \tag{A23}$$

where $t_B = 0.16$ mils, $t_M = 1.10$ mils, $E_M = 0.5 \times 10^6$ psi, $E_B = 60 \times 10^6$ psi, $\nu_B = 1/4$, and $\nu_M = 1/3$.

It is noted that the maximum tensile stress which develops on the matrix-boron interface during loading is

$$\sigma_M = \frac{E_M}{1 - \nu_M^2} \frac{2B}{t_M} \tag{A24}$$

Equation (A13) is used to determine B in this formula for σ_M. When λ/λ_w is given by Equation (A23), σ_M is

$$\sigma_M = 3.27 \times 10^5 \alpha_w \frac{A}{t_B} \left[(0.1542 \frac{\lambda}{t_B})^{-2} + (0.1542 \frac{\lambda}{t_B})^2 - 2\alpha_w \right]^{-1} \tag{A25}$$

Antisymmetric Case:

In this case the matrix is subjected to shearing strain when y_1 occurs. That shearing strain is

$$\gamma_M = \left(1 + \frac{t_B}{t_M}\right) y_1' \tag{A26}$$

The shearing stresses will be constant through the thickness;

$$\tau_M = G_M \gamma_M \tag{A27}$$

The differential element shown in Figure 13 is of thickness $t_B + t_M$, the repeating element of the composite. The above shearing stresses act on each side of the repeating element, but in opposite

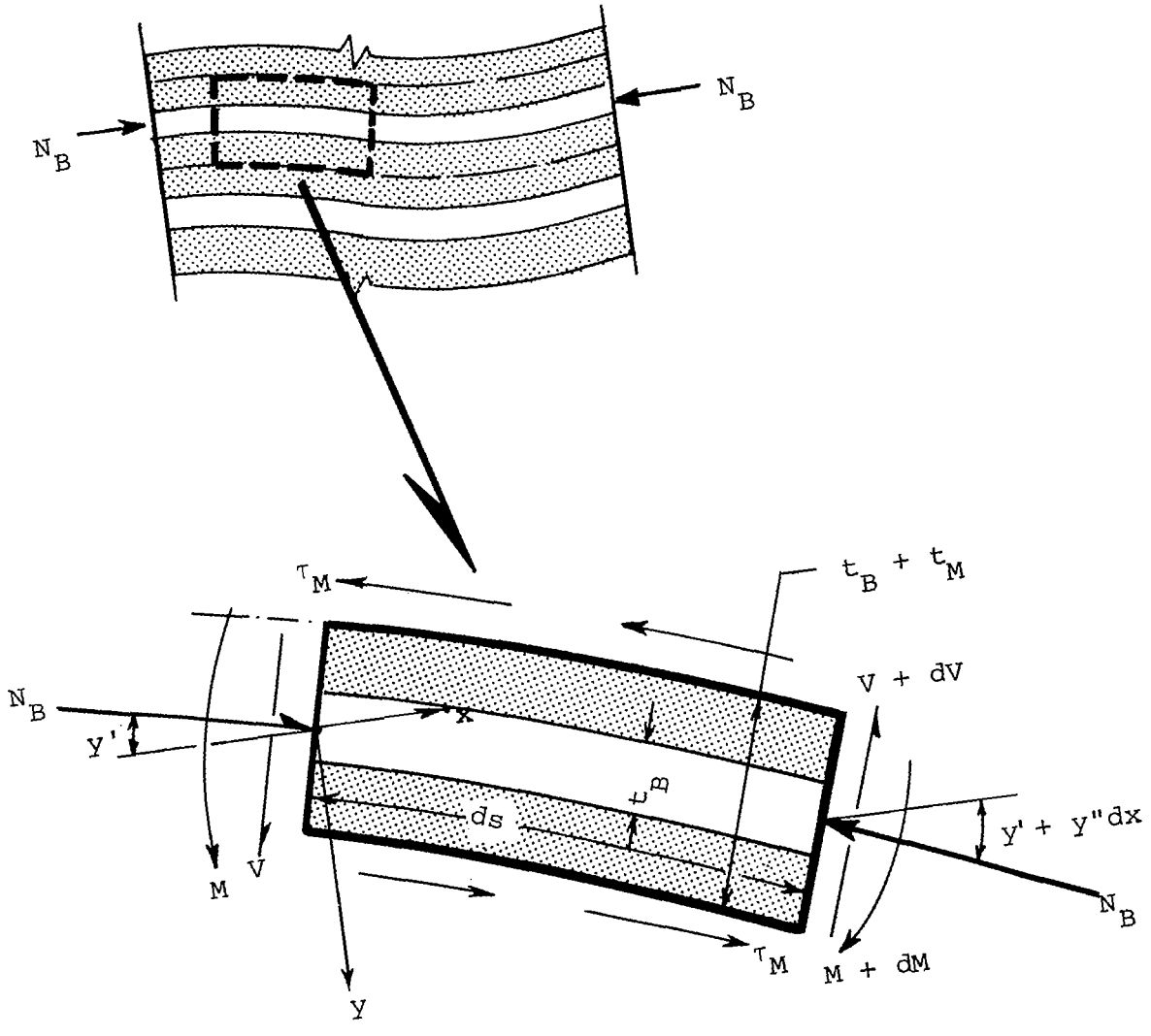

Figure 13. Differential Element of Repeating Sections of Layered Composite

directions. For equilibrium, the forces on the differential element in Figure 13 must satisfy the following equations:

$$M_B' - G_M (t_B + t_M) \gamma_M - V = 0 \tag{A28}$$

and

$$V' + N_B y'' = 0 \tag{A29}$$

Therefore, the above two equations along with Equation (A26) combine as

$$M_B'' + N_B (y_o'' + y_1'') - G_M t_M \left(1 + \frac{t_B}{t_M}\right)^2 y_1'' = 0 \tag{A30}$$

By substituting in Equation (A30) the expressions for M_B, y_o, and y_1 as defined above, the following relationship between B and A is obtained:

$$\frac{B}{A} = \frac{N_B}{D_B\left(\frac{\pi}{\lambda}\right)^2 + G_M t_M \left(1 + \frac{t_B}{t_M}\right)^2 - N_B} \tag{A31}$$

The critical value of N_B is that which causes B to increase indefinitely. Therefore, when minimized with respect to wavelength,

$$N_{B_{CR}} = G_M t_M \left(1 + \frac{t_B}{t_M}\right)^2 \tag{A32}$$

for $\lambda = \infty$. From the rule of mixtures,

$$N_B = \frac{N_C}{1 + \frac{t_M}{t_B}\frac{E_M}{E_B}} \tag{A33}$$

Therefore,

$$N_{C_{CR}} = G_M t_M \left(1 + \frac{t_B}{t_M}\right)\left(1 + \frac{t_M}{t_B}\,\frac{E_M}{E_B}\right) \tag{A34}$$

This result differs from that of Reference 2 for $N_{C_{CR}}$ by the factor $1 + \frac{t_M}{t_B}\,\frac{E_M}{E_B}$ because the strain energy in compression of the matrix during buckling was neglected in that work.

By using the definition $\alpha_s = {}^{N_C}\Big/{}_{N_{C_{CR}}}$, Equation (A31) becomes

$$\frac{B}{A} = \frac{\alpha_s}{1 + \dfrac{D_B\left(\frac{\pi}{\lambda}\right)^2}{G_M t_M \left(1 + \frac{t_B}{t_M}\right)^2} - \alpha_s} \tag{A35}$$

This expression for A/B can now be substituted in Equation (A17) to determine δ and the result can be substituted into Equation (A20) to obtain the following expression for $\overline{E}_B/E_B$:

$$\frac{\overline{E}_B}{E_B} = \frac{1}{1 + \frac{E_B}{G_M}\,\frac{t_B}{t_M}\,\varphi_s} \tag{A36}$$

where

$$\varphi_s = \frac{\frac{\pi^2 A^2}{2\lambda^2}\left\{1 + \frac{D_B}{G_M t_M}\left[\frac{\pi}{\lambda\left(1 + \frac{t_B}{t_M}\right)}\right]^2\right\}}{\left(1 + \frac{t_B}{t_M}\right)^2\left\{1 + \frac{D_B}{G_M t_M}\left[\frac{\pi}{\lambda\left(1 + \frac{t_B}{t_M}\right)}\right]^2 - \alpha_s\right\}^2} \tag{A37}$$

When $\alpha_s = 0$, and its terms are rearranged, φ_s becomes φ_o and is

$$\varphi_o = \frac{\frac{\pi}{2}^2 \left(\frac{A}{t_B}\right)^2}{\left(\frac{\lambda}{t_B}\right)^2 \left(1 + \frac{t_B}{t_M}\right)^2 + \frac{\pi^2}{12\,(1-\nu_B^2)} \frac{E_B}{G_M} \frac{t_B}{t_M}} \tag{A38}$$

The maximum shearing stress that develops in the matrix during loading is

$$\tau_M = G_M \left(1 + \frac{t_B}{t_M}\right) \left(\frac{\pi}{\lambda}\right) B \tag{A39}$$

By substituting from Equation (A35) for B, τ_M becomes

$$\tau_M = \frac{G_M \left(1 + \frac{t_B}{t_M}\right) \left(\frac{A}{t_B}\right) \left(\frac{t_B}{\lambda}\right) \pi \alpha_s}{1 - \alpha_s + \left(\frac{t_B}{\lambda}\right)^2 \frac{\pi^2}{12} \frac{E_B}{G_M} \frac{t_B}{t_M} (1-\nu_B^2)^{-1} \left(1 + \frac{t_B}{t_M}\right)^{-2}} \tag{A40}$$